RSC Advances

PAPER

View Article Online
View Journal | View Issue

Cite this: *RSC Adv.*, 2023, **13**, 10508

Yellow emissive nitrogen-doped carbon dots as a fluorescence probe for the sensitive and selective detection of silver ions†

Juan Hou, *[a] Xu Gao, [b] Siqi Bao,[a] Shuqi Liu[b] and Guang Yang *[b]

Received 24th February 2023
Accepted 28th March 2023

DOI: 10.1039/d3ra01259j

rsc.li/rsc-advances

In this work, yellow emissive carbon dots (Y-CDs) were prepared *via* a simple hydrothermal method using catechol and hydrazine hydrate as the carbon and nitrogen sources, respectively. The average particle size was 2.99 nm. The Y-CDs demonstrate excitation-dependent emission properties, and the maximum emission wavelength is 570 nm at E_x = 420 nm. The fluorescence quantum yield is calculated to be 28.2%. Ag^+ could quench the fluorescence of Y-CDs with high selectivity. The quenching mechanism was further explored by various characterization techniques. A sensitive fluorescent probe for Ag^+ detection was established based on Y-CDs with a linear range of 3–300 μM. The detection limit was calculated to be 1.1 μM. The proposed method shows satisfactory results in real water samples without interference by coexistence.

Introduction

Silver, as an important kind of toxic heavy metal, has been widely utilized in various application fields, such as catalytic engineering, water purification, jewellery manufacturing, and electrical materials.[1–3] However, the improper disposal of Ag^+ would inevitably cause an alarming rise in environmental pollution and pose a threat to the ecosystem. In addition, Ag^+ can combine with some proteins, metabolites and enzymes in the human body, resulting in enzyme inactivation, cardiac hypertrophy, skin lesions and other diseases. Therefore, it is of great importance to develop a fast and sensitive detection method for Ag^+. At present, the main methods for the determination of Ag^+ include atomic absorption method, electrochemical analysis,[4] Raman analysis,[5] colorimetric detection,[6] *etc.* These methods in practical applications are often limited by complex equipment, less sensitivity, being time-consuming and cumbersome operation.[7] Fluorescence detection is proved to be an effective method for metal ion detection in food and environmental samples owing to the advantages of simple operation, rapid response, low cost and good selectivity.[8–10]

Recently, carbon dots (CDs) have attracted much consideration due to their outstanding features such as fast synthetic route, easy surface functionalization, environmental friendliness, low cost and good fluorescence properties, which can be used as a new type of fluorescent materials to replace quantum dots and organic dyes in the field of sensing.[11–14] Heteroatomic doping could induce the Fermi level to move up and greatly improve the photoluminescence performance of CDs, thereby expanding the application scope.[15–18] Doping CDs have been applied to the detection of metal ions, small organic molecules and proteins.[18,19] However, most reported CDs display blue emissions, which cannot be distinguished from the largely blue naturally occurring autofluorescence.[20] Significant efforts have been made to make the fluorescence redshift to long-wavelengths, but the preparations always need long reaction times and severe synthetic conditions. Additionally, the Ag^+ detection is rarely reported.

As illustrated in Scheme 1, we proposed a simple hydrothermal method to fabricate N-doped CDs with bright yellow emissions (Y-CDs). A Y-CDs based fluorescence probe was established to detect Ag^+ in a real water sample with a quenching response of 3–300 μM under optimum detection conditions. The characterization and quenching mechanism were investigated in detail.

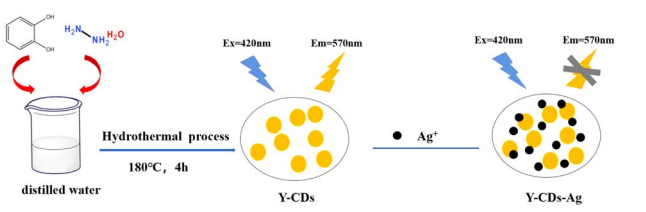

Scheme 1 Schematic diagram of Y-CDs preparation and the detection process of Ag^+.

[a]*Key Laboratory of Applied Chemistry and Nanotechnology at Universities of Jilin Province, Changchun University of Science and Technology, Changchun 130022, China. E-mail: houjuan0503@126.com*

[b]*Department of Chemistry, Chemical Engineering and Resource Utilization, Northeast Forestry University, Harbin 150040, China. E-mail: guangyang@nefu.edu.cn*

† Electronic supplementary information (ESI) available. See DOI: https://doi.org/10.1039/d3ra01259j

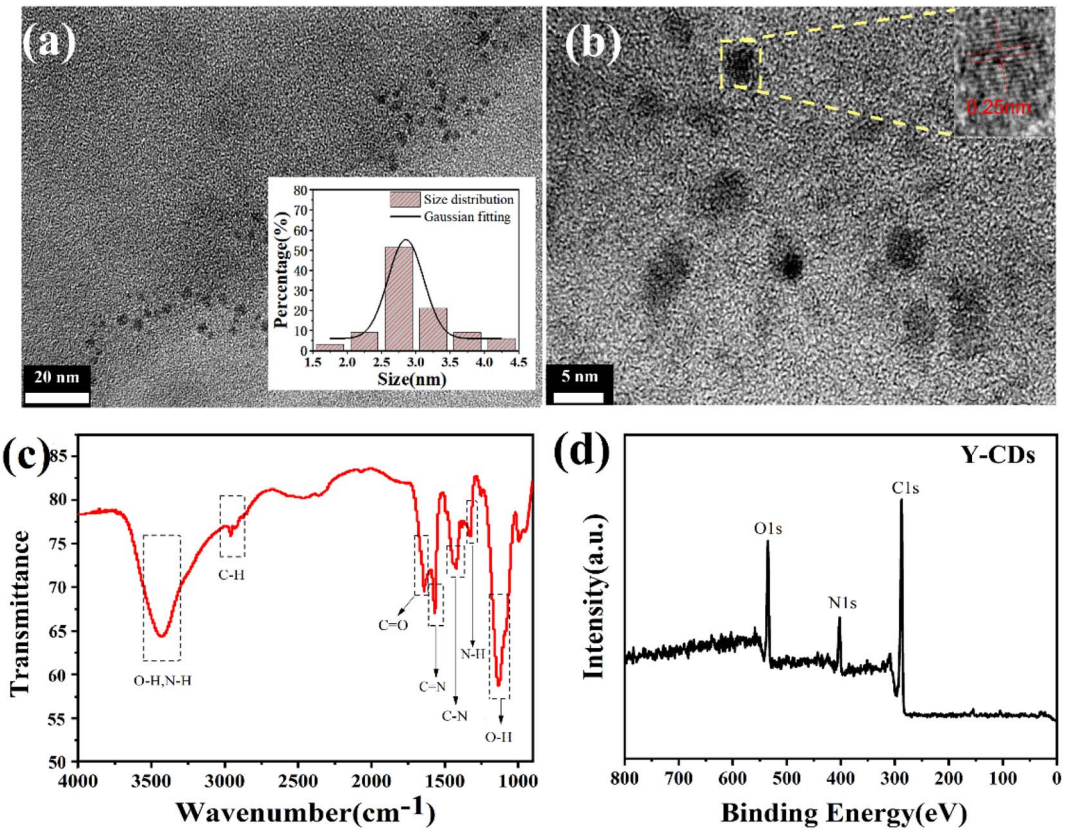

Fig. 1 (a) TEM image of Y-CDs; inset is the size distribution based on statistical analysis of 100 particles; (b) HRTEM image of the Y-CDs; (c) FTIR spectrum of Y-CDs; (d) full survey XPS spectrum of Y-CDs.

Experimental section

Y-CDs were prepared *via* a simple hydrothermal route. Briefly, 0.5534 g of catechol and 2 mL of hydrazine hydrate were added to 30 mL distilled water. The mixture was ultrasonicated for 5 min and transferred to a 50 mL Teflon reaction vessel. After heating at 180 °C for 4 h, the obtained brown Y-CDs solution was purified by dialysis (500 Da) and dried at 60 °C by a rotary evaporator to obtain Y-CDs powders. Aqueous CDs (500 μg mL^{-1}) solutions were obtained by redispersion the Y-CDs powders in DI water, and then stored in refrigerator at 4 °C before analysis.

For a typical procedure for Ag^+ detection, 500 μL of Y-CDs solution (500 μg mL^{-1}), 3 mL BR buffer solution (pH = 7) and 100 μL of Ag^+ solutions with different concentrations were mixed with distilled water to 10 mL. After 10 min of incubation, the fluorescence spectra were recorded at an excitation wavelength of 420 nm. During the detection, the excitation and emission slits were set at 10 nm. To study the selectivity of Y-CDs to Ag^+, the fluorescence response to various metal ions, small molecules and anions was recorded under the same conditions.

Real water samples were collected from river water, underground water and tap water and filtered using a 0.22 μm filter. The initial Ag^+ concentrations in real water samples were obtained by standard addition method and compared with the data by ICP-MS analysis.

Results and discussion

The transmission electron microscopy (TEM) image in Fig. 1a shows the morphology and size of the Y-CDs. The as-prepared Y-CDs are spherical and uniformly distributed with average sizes of approximately 2.99 nm (based on statistical analysis of 100 particles). The high-resolution TEM image inset in Fig. 1b reveals obvious lattice fringes with a spacing of 0.25 nm, which is consistent with the (1 0 0) diffraction plane of graphite.[21] The Fourier transform infrared (FTIR) spectrum is shown in Fig. 1c. The characteristic absorption peak at 3429 cm^{-1} represents the stretching vibration of O–H and N–H groups.[22] The absorption peak at 2958 cm^{-1} is the stretching vibration peak of C–H.[23] The characteristic peak at 1650 cm^{-1} indicates the existence of C=O and peak at 1553 cm^{-1} represents the C=N bonds of imine groups.[24] Peaks at 1450 cm^{-1}, 1375 cm^{-1} and 1125 cm^{-1} represent the bending vibrational modes of C–N, N–H and O–H groups.[25] To further ascertain the elemental composition and chemical bonds of Y-CDs, XPS analysis is conducted as shown in Fig. 1d. The full survey XPS spectrum demonstrates that C, N and O coexisted in the Y-CDs at 284.35, 399.19 and 531.4 eV with corresponding contents of 69.53%, 12.98% and 17.49%, respectively. Deconvolution of C_{1s} can be divided into four

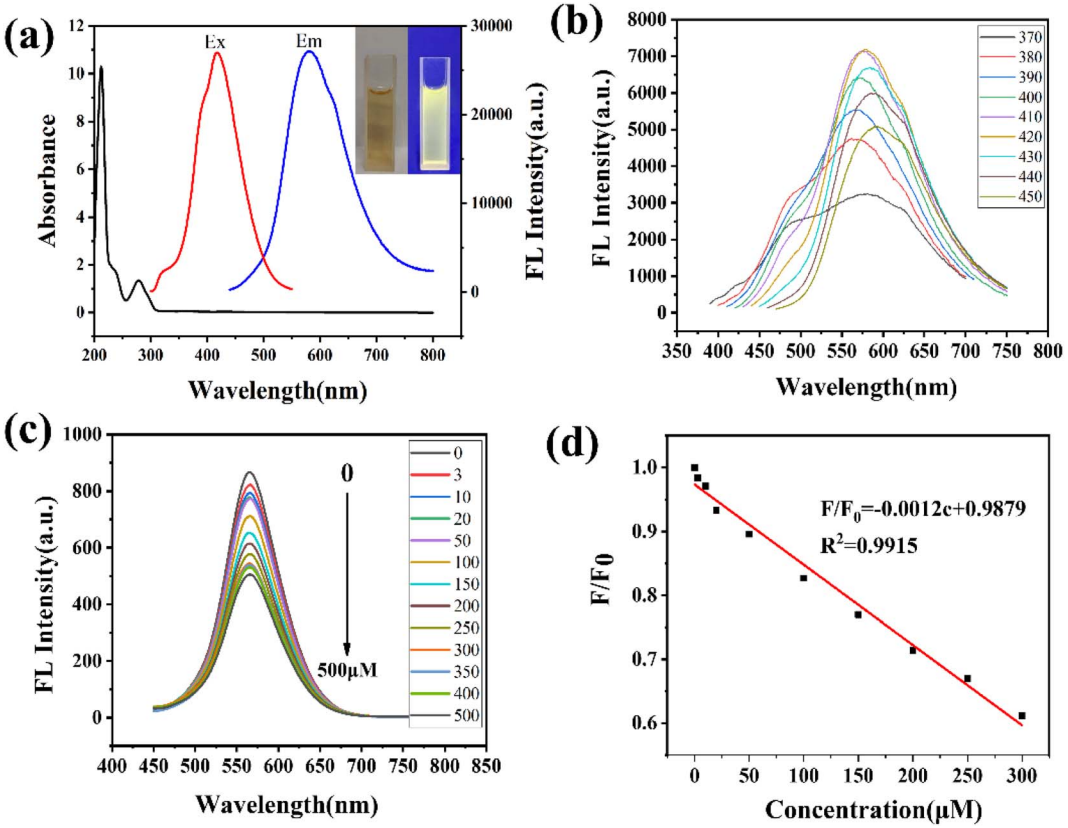

Fig. 2 (a) UV-vis absorption spectrum and fluorescence spectra of Y-CDs, the inset shows the photographs of Y-CDs solution in daylight (left) and UV lamp (right); (b) fluorescence emission spectra at λ_{ex} = 370–450 nm; (c) the fluorescence spectra of Y-CDs solution with different Ag^+ concentration; (d) linear relationship between F/F_0 and Ag^+ concentration (3–300 μM).

peaks, corresponding to C=C (284.4 eV), C–N (286.2 eV), C=O (287.7 eV) and C=N/O–C=O (288.1 eV), respectively (Fig. S1a†).[24] Fig. S1b† shows the high-resolution spectrum of N_{1s}. The peaks at 398.4 eV, 399.3 eV and 400.2 eV are related to imine N, C–N and N–(C_3), respectively,[17] which proves the successful doping of N element. The O_{1s} spectrum in Fig. S1c† can be resolved into two components of C=O (531.2 eV) and C–OH (532.7 eV).[26] The FTIR and XPS results demonstrate rich carboxyl and hydroxyl groups on the surface, making the Y-CDs with good water solubility.

The optical properties are characterized by UV-vis and fluorescence spectra. As shown in Fig. 2a, the Y-CDs exhibit an obvious characteristic absorption peak at 278 nm, which can be ascribed to the π–π* transition of C=C in the aromatic structure.[27] The Y-CDs solution is light brown under sunlight, while it emits bright yellow fluorescence under a UV beam of 365 nm. The fluorescence spectra demonstrate the maximum emission intensity of 570 nm under 420 nm excitation. The emission wavelength redshifts a longer wavelength as the excitation wavelength increases from 420 nm to 580 nm, which is attributed to the various emissive traps on the surface (Fig. 2b).[27] The fluorescence quantum yield of Y-CDs is calculated to be 28.2%. The Y-CDs were stable in high concentrations of NaCl solution (0–2 M), under continuous UV illustration (100 min) and long-time storage (20 days), indicating good chemical stability and photobleaching resistance (Fig. S2†). Moreover, the Y-CDs showed obvious pH sensitive emission properties, which is due to the protonation and deprotonation of surface functional groups. The maximum fluorescence intensity was observed at pH = 7 (Fig. S3†).

The extensive quenching performance of Y-CDs could be observed upon the addition of Ag^+ (Fig. 2c). To determine the selectivity, the influence of different metal ions, small molecules and anions at the same concentration was investigated. As shown in Fig. S4,† Cu^{2+} demonstrates obvious quenching effect on the fluorescence, whereas other ions and molecules showed negligible changes in fluorescence (Fig. S4†). EDTA, as a coordination agent for Cu^{2+}, was added to the system, which might effectively eliminate the interference. As shown in Fig. S5,† at pH = 7, Ag^+ demonstrated the largest quenching performance and Cu^{2+} may exert some interference on Ag^+ detection. But after the introduction of EDTA, the quenching effect of Cu^{2+} could be ignored. Meantime, the co-existing metal ions also showed little influence on the Y-CDs/Ag^+ system (Fig. S6†). Thus, Y-CDs could be used as a fluorescence probe for the selective detection of Ag^+. The fluorescence quenching reached equilibrium after 8 min (Fig. S7†). Therefore, 10 min was selected as the incubation time. The effect of Ag^+ at different concentrations ranging 0–500 μM on the fluorescence intensities was investigated in detail. A good linear correlation was

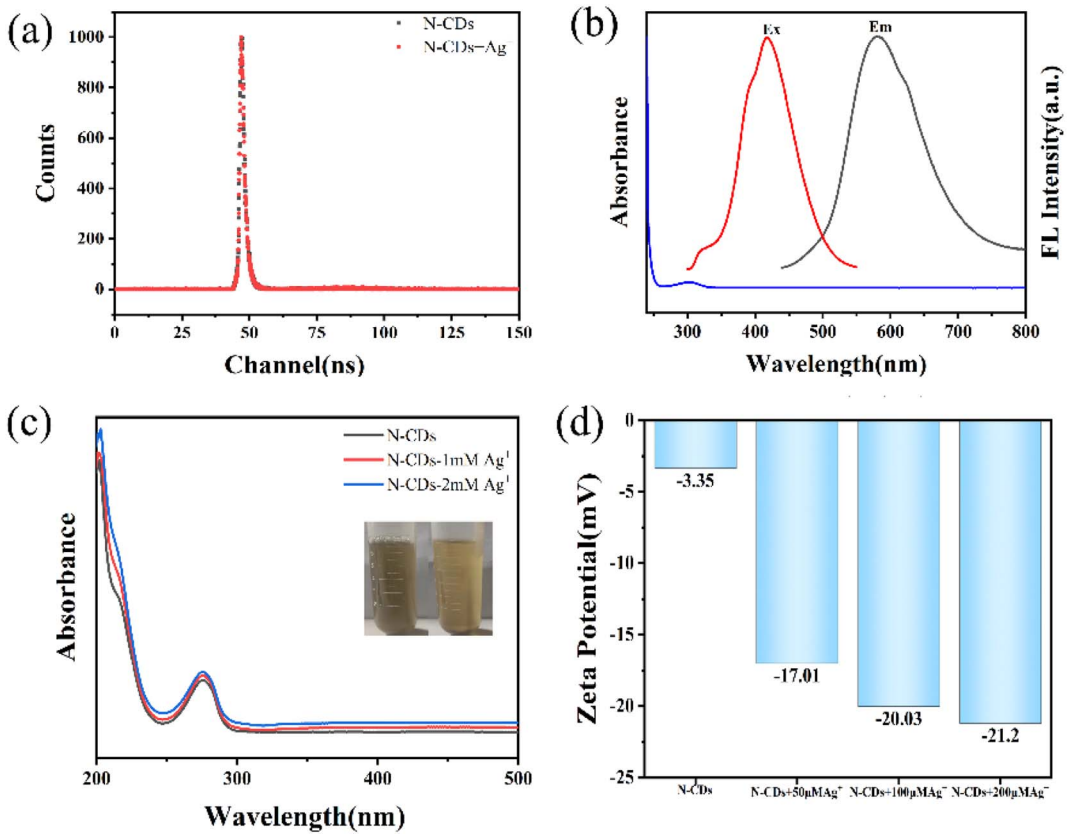

Fig. 3 (a) Fluorescence lifetime of Y-CDs before and after Ag^+ addition; (b) UV-vis absorption spectrum of Ag^+ and excitation and emission spectrum of N-CDs; (c) UV-vis absorption spectrum of N-CDs with different concentrations of Ag^+ (illustration shows the flocculation effect of Ag^+), (d) zeta potential change after addition of Ag^+.

observed over the concentration of Ag^+ in the range of 3–300 μM (Fig. 2d). The regression equation is as follows:

$$F/F_0 = -0.0012c + 0.9879$$

The detection limit of Ag^+ was calculated to be 1.1 μM based on a 3δ/slope, which is comparable with the sensor reported in other literature (Table S1†).

The mechanism of quenching performance by Ag^+ was further investigated. As shown in Fig. 3a, the average fluorescence lifetime of Y-CDs changed from 1.362 ns to 1.424 ns after the addition of Ag^+, which is not consistent with dynamic quenching.[29] Ag^+ showed a UV absorption band at 302 nm, while the excitation peak of Y-CDs was located at 420 nm (Fig. 3b). The absorption of Ag^+ does not overlap with the excitation and emission peaks of Y-CDs, thus eliminating the IFE quenching mechanism. The UV-vis spectra of Y-CDs did not change significantly with the addition of Ag^+, and PET (photo-induced electron transfer) and complex formation were excluded (Fig. 3c).[28,29] The zeta potential value of Y-CDs gradually decreases with the addition of different concentrations of Ag^+ (Fig. 3d). The peak at 1553 cm^{-1} derived from C=N disappears and the FTIR peaks of N–H groups slightly shift (Fig. S8†). Black flock-like precipitation appears at the bottom of the bottle. Therefore, the quenching mechanism may be derived from the imine group on the surface of Y-CDs oxidized or shielded by Ag^+. Thus, Ag^+ is reduced to Ag^0 nanoparticles

Table 1 Determination of Ag^+ in real samples

Samples	Detected/μM	Detected by ICP-MS/μM	Spiked/μM	Found/μM	Recovery (%)	RSD (n = 3)
1	3.3	3.6	5	8.498	104.0	4.2
			50	52.62	98.64	3.4
2	Not detected	Not detected	10	9.32	93.20	2.2
			100	94.91	94.91	3.9
3	Not detected	Not detected	20	21.18	105.9	2.6
			300	292.42	97.47	1.1

and attached to the surface of Y-CDs, which leads to fluorescence quenching.[1,30]

To verify the feasibility of the Y-CDs based fluorescent probe in practical applications, we applied it to the determination of Ag^+ in real water samples. For this purpose, river water, underground water and tap water were collected. Prior to the fluorescence experiments, the samples were filtered through a 0.22 μm microporous filter. The results are shown in Table 1. The detection results were approximately identical with that measured by ICP-MS. The recoveries of the spiked samples ranged from 93.20% to 105.9%, and the RSD was lower than 4.2%. Despite the potential interference from the coexistence, the proposed method indicates good sensitivity and accuracy.

Conclusions

In this work, N doped CDs with bright yellow fluorescence (Y-CDs) were synthesized in one step by a hydrothermal method. The prepared Y-CDs demonstrate good chemical and optical stability. The imine groups on the surface of Y-CDs may be oxidized or shielded by Ag^+, so that Ag^+ was reduced to Ag nanoparticles and attached to the surface of Y-CDs, resulting in significant fluorescence quenching. The quenching performance displayed a linear relationship in the range of 3–300 μM, and the detection limit was 1.1 μM. Subsequently, the proposed method was applied to the quantitative detection of Ag^+ in real water samples with satisfactory recoveries of 93.20–105.9%, indicating good applicability in practical analysis.

Author contributions

Juan Hou: methodology, data analysis, writing, investigation; Xu Gao: experiment conduction, investigation, data curation; Siqi Bao: data analysis, experiment conduction, review; Shuqi Liu: experiment conduction, investigation; Guang Yang: resources, supervision, review and editing.

Conflicts of interest

There are no conflicts to declare.

Acknowledgements

We gratefully acknowledge the support from the Joint Fund Project of the Natural Science Foundation of Jilin Province (YDZJ202101ZYTS076) and the National Natural Science Foundation of China (NSFC, No. 21804017). The authors also would like to thank Shiyanjia Lab (**https://www.shiyanjia.com**) for the assistance with testing.

Notes and references

1 G. Liu, C. Xuan, D.-Q. Feng, D. Hua, T. Liu, G. Qi and W. Wang, *Anal. Methods*, 2017, **9**, 5611–5617.
2 J. Guo, S. Ye, H. Li, J. Song and J. Qu, *Dyes Pigm.*, 2020, **183**, 108723.
3 Q. Long, Y. Wen, H. Li, Y. Zhang and S. Yao, *J. Fluoresc.*, 2017, **27**, 205–211.
4 G. Xu, G. Wang, X. He, Y. Zhu, L. Chen and X. Zhang, *Analyst*, 2013, **138**, 6900–6906.
5 E. Tan, P. Yin, X. Lang, X. Wang, T. You and L. Guo, *Analyst*, 2012, **137**, 3925–3928.
6 Y.-M. Sung and S.-P. Wu, *Sens. Actuators, B*, 2014, **197**, 172–176.
7 N. Sohal, B. Maity and S. Basu, *ACS Appl. Nano Mater.*, 2020, **3**, 5955–5964.
8 X. Ran, H. Sun, F. Pu, J. Ren and X. Qu, *Chem. Commun.*, 2013, **49**, 1079–1081.
9 Y. Zhang, A. Ye, Y. Yao and C. Yao, *Sensors*, 2019, **19**, 247.
10 A. Kundu, B. Maity and S. Basu, *ACS Biomater. Sci. Eng.*, 2022, **8**, 4764–4776.
11 X. T. Zheng, A. Ananthanarayanan, K. Q. Luo and P. Chen, *Small*, 2015, **11**, 1620–1636.
12 C. Long, Z. Jiang, J. Shangguan, T. Qing, P. Zhang and B. Feng, *Chem. Eng. J.*, 2021, **406**, 126848.
13 P. Lesani, G. Singh, Z. Lu, M. Mirkhalaf, E. J. New and H. Zreiqat, *Chem. Eng. J.*, 2022, **433**, 133668.
14 P. Lesani, Z. Lu, G. Singh, M. Mursi, M. Mirkhalaf, E. J. New and H. Zreiqat, *Nanoscale*, 2021, **13**, 11138–11149.
15 X. Zhai, P. Zhang, C. Liu, T. Bai, W. Li, L. Dai and W. Liu, *Chem. Commun.*, 2012, **48**, 7955–7957.
16 R. Hu, L. Li and W. J. Jin, *Carbon*, 2017, **111**, 133–141.
17 S. Yang, J. Sun, X. Li, W. Zhou, Z. Wang, P. He, G. Ding, X. Xie, Z. Kang and M. Jiang, *J. Mater. Chem. A*, 2014, **2**, 8660.
18 N. Sohal, S. Basu and B. Maity, *Microchem. J.*, 2023, **185**, 108287.
19 N. Sohal, B. Maity and S. Basu, *RSC Adv.*, 2021, **11**, 25586–25615.
20 P. Lesani, A. H. M. Hadi, Z. Lu, S. Palomba, E. J. New and H. Zreiqat, *Commun. Mater.*, 2021, **2**, 108.
21 Y. Z. Fan, Y. Zhang, N. Li, S. G. Liu, T. Liu, N. B. Li and H. Q. Luo, *Sens. Actuators, B*, 2017, **240**, 949–955.
22 W. Lu, X. Gong, M. Nan, Y. Liu, S. Shuang and C. Dong, *Anal. Chim. Acta*, 2015, **898**, 116–127.
23 J. Hou, T. Zhou, L. Wang, P. Zhang and L. Ding, *Sens. Actuators, B*, 2016, **230**, 615–622.
24 Q. Xu, P. Pu, J. Zhao, C. Dong, C. Gao, Y. Chen, J. Chen, Y. Liu and H. Zhou, *J. Mater. Chem.*, 2015, **3**, 542–546.
25 B. Shi, Y. Su, L. Zhang, M. Huang, R. Liu and S. Zhao, *ACS Appl. Mater. Interfaces*, 2016, **8**, 10717–10725.
26 Y.-L. Zhang, L. Wang, H.-C. Zhang, Y. Liu, H.-Y. Wang, Z.-H. Kang and S.-T. Lee, *RSC Adv.*, 2013, **3**, 3733–3738.
27 S. Pei, J. Zhang, M. Gao, D. Wu, Y. Yang and R. Liu, *J. Colloid Interface Sci.*, 2015, **439**, 129–133.
28 F. Zu, F. Yan, Z. Bai, J. Xu, Y. Wang, Y. Huang and X. Zhou, *Microchim. Acta*, 2017, **184**, 1899–1914.
29 L. Wang, Y. Bi, J. Hou, H. Li, Y. Xu, B. Wang, H. Ding and L. Ding, *Talanta*, 2016, **160**, 268–275.
30 T. Liu, J. X. Dong, S. G. Liu, N. Li, S. M. Lin, Y. Z. Fan, J. L. Lei, H. Q. Luo and N. B. Li, *J. Hazard. Mater.*, 2017, **322**, 430–436.